Volume 14
Number 6
21 March 2024
Pages 1377–1692

Catalysis Science & Technology

rsc.li/catalysis

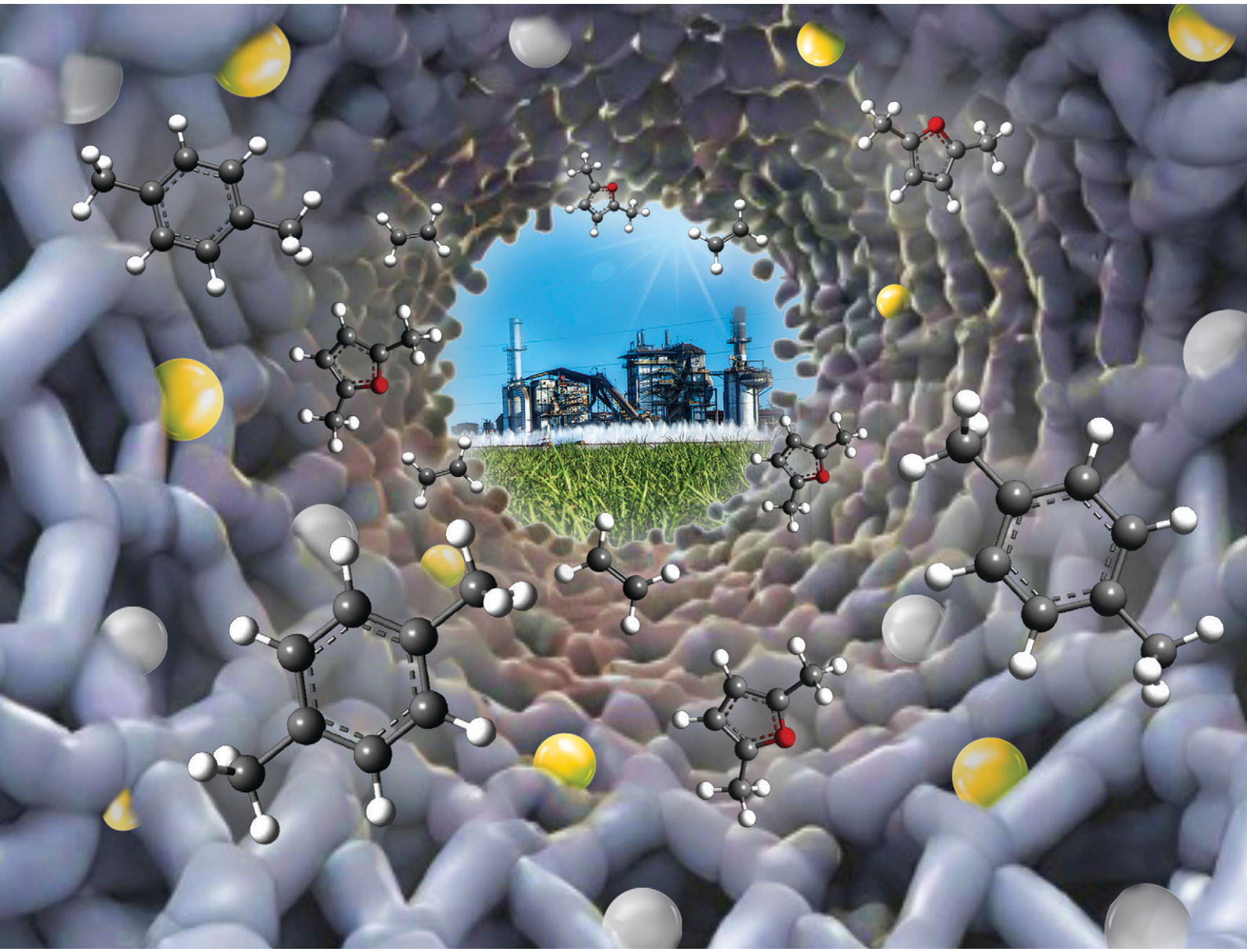

ISSN 2044-4761

ROYAL SOCIETY OF CHEMISTRY

PAPER

Verónica R. Elías, Marcelo E. Domine *et al.*
From biomass-derived furans to aromatic compounds: design of Al–Nb-SBA-15 mesoporous structures and study of their acid properties on catalytic performance

Catalysis Science & Technology

ROYAL SOCIETY OF CHEMISTRY

PAPER

View Article Online
View Journal | View Issue

Cite this: *Catal. Sci. Technol.*, 2024, **14**, 1488

From biomass-derived furans to aromatic compounds: design of Al–Nb-SBA-15 mesoporous structures and study of their acid properties on catalytic performance†

Verónica R. Elías,*[a] Gabriel O. Ferrero,[a] Madalina G. Idriceanu,[b] Griselda A. Eimer[a] and Marcelo E. Domine *[b]

Renewable aromatics compounds (*i.e.* BTXs) are interesting, useful and much desired chemicals for industry due to the lack or difficulty to find available non-fossil feedstocks capable to produce these aromatics in good yields. Therefore, the aromatization reaction of biomass-derived furans is a valuable strategy for a sustainable production of aromatic compounds. In this work, modified SBA-15 mesoporous silicates with enhanced acid properties were successfully synthetized by a one-pot method, directly incorporating the metal precursor (Nb, W, Ga, Zr, Al) in the synthesis gel. The solids were characterized by different techniques, such as XRD, TEM, ICP, N_2 physisorption, FT-IR of adsorbed pyridine and NH_3-TPD, among others. The catalytic performance of mesoporous materials was tested in the Diels–Alder (DA) aromatization reaction using 2,5-DMF as a diene and ethylene as a dienophile for the selective production of *p*-xylene (*p*-xy). Among the mono-metallic solids (modified with Nb, W, Ga, Zr or Al) showing Lewis (Le) acidity, only those that also present Brønsted (Br) sites showed activity in the aromatization reaction, appearing Al(*x*)–S as the most selective catalyst for the *p*-xy production. Then, Br acidity in bi-metallic solids was ensured by co-incorporating Al in the structure, showing Al–Nb-SBA-15 – materials the best catalytic performance. For these solids, the *p*-xy yield showed a strong dependence with the metal content and the moderate strength Br/Le acid sites ratio. Optimization of the composition of Al–Nb-SBA-15 catalyst and the reaction conditions allowed reaching a *p*-xy yield even higher than that observed for previous reported reference catalyst (*i.e.* H-ZSM-5). It was demonstrated that the type of metals (Al and Nb) incorporated in SBA-15 provides an adequate combination of Br and Le acid sites of moderate strength and homogeneously distributed on the solid (low surface density of acid sites), which together with the high accessibility offered by the mesoporous material, are features to be considered for the aromatic production. The observed activity for catalysts with both Le and Br sites was mainly attributed to their ability to retard side reactions, such as oligomerization and alkylation by means of the effective cycloaddition of 2,5-DMF with ethylene in Le sites, in addition to the dehydrative aromatization reaction allowed by the presence of Br acidity.

Received 8th January 2024,
Accepted 21st January 2024

DOI: 10.1039/d4cy00033a

rsc.li/catalysis

Introduction

With the aim to contribute to the sustainability of chemical processes, the scientific researchers around the world are continually working on the development of new catalytic materials for the valorization of renewable raw materials, specifically for processing biomass-derived compounds.[1,2] Among these, furan compounds emerge as intermediate substances from lignocellulosic sources that can be used as platform molecules to obtain more valuable products.[3,4] Examples of these furanic type compounds are: furfural or FAL (obtained *via* selective dehydration of C5 sugars),[5] 5-hydroxymethyl furfural or 5-HMF (synthesized *via* selective dehydration of fructose),[6] furfuryl alcohol or FOL (attained *via* selective hydrogenation of FAL),[7] furan and 2-methylfuran or 2-MF (produced by selective hydrogenation of furfural),[3] 2,5-dimethylfuran or 2,5-DMF (produced by selective reduction of 5-HMF),[8] among others. These furanic

[a] *Centro de Investigación y Tecnología Química (CITeQ) UTN-CONICET, Maestro López esq. Cruz Roja s/n, Ciudad Universitaria, 5003, Córdoba Capital, Argentina. E-mail: velias@frc.utn.edu.ar*
[b] *Instituto de Tecnología Química (ITQ, UPV-CSIC), Universitat Politècnica de València, Consejo Superior de Investigaciones Científicas, Avda de los Naranjos s/n, 46022, Valencia, Spain. E-mail: mdomine@itq.upv.es*

† Electronic supplementary information (ESI) available. See DOI: https://doi.org/10.1039/d4cy00033a

compounds could be used as starting reactants to get a wide range of valuable compounds for chemical industry, by covering substances as furfuryl-dicarboxylic acid (FDCA) used as monomer for polymers synthesis,[9] tetrahydrofuran (THF) and derivatives commonly used as solvents and additives for polymers,[3] tetrahydrofurfuryl alcohol (THFOL) and their derived alkyl-ethers useful as components and additives for renewable fuels,[10] and even aromatic (BTXs) compounds commonly used in petrochemical industry.[2]

In this sense, aromatic hydrocarbons are a family of compounds widely used in several industrial processes involving the production of plastics, agrochemicals, fragrances, *etc.* *p*-xylene (*p*-xy) belongs to this type of substances and has multiple applications as solvent, for fuels formulations, polymers fabrication, *etc.*[11,12] Nevertheless, it is usually obtained from petroleum-based carbon resources.[13,14] Looking for a renewable and sustainable alternative for its production it has been proposed an interesting strategy based on Diels–Alder (DA) reaction that using 2,5-DMF from biomass as a diene and short chain olefins as dienophiles, produces a cycloadduct that after dehydration becomes an aromatic molecule.[15–18] This alternative method for the aromatic production involves 2 stages (see Scheme 1) and could be enhanced by the presence of heterogeneous catalysts. Nevertheless, two kind of acid sites must be present in the catalyst structures. In the first stage, the formation of the intermediate cycloadduct is enhanced by the presence of Lewis (Le) sites, meanwhile in the second stage, the aromatic is formed from the dehydration reaction of the cycloadduct which could be produced over Brønsted (Br) sites.[19]

Some solids have been tested as catalysts for this reaction such as phosphotungstic acid (HPW) and silicotungstic acid (HSiW) supported on various oxides, SiO_2, Al_2O_3, TiO_2, ZrO_2. It was observed that HPA/SiO_2 activity is considerably greater than that for the HPAs supported on Al_2O_3, ZrO_2, and TiO_2 and this behavior was assigned to their higher acid site density and stronger Br acidity.[20] Zirconium phosphates (ZrP) grafted on ordered mesoporous silicas such as KIT-6 and SBA-15 and supported on not ordered fumed SiO_2 were also tested in the *p*-xy production. The ordered supports modified with ZrP revealed a higher aromatic production rate probably due to the presence of homogenously dispersed acidic sites on a large surface which provokes an increased overall acidity, compared to that of non-ordered silica support whose acid sites are densely distributed on a smaller surface.[11]

The use of H-beta and H-Y zeolites for the *p*-xy synthesis with 90% yield by cycloaddition of biomass-derived 2,5-DMF and ethylene has been reported. Nevertheless, with these zeolites a significant loss of carbon occurs during reaction mainly due to the formation of dimers and larger oligomers, thus conducting to large amounts of coke deposited on solids which provokes a rapid catalytic deactivation.[18] On the contrary, when Lewis acid catalysts as $AlCl_3$ were combined with Na–Y zeolite for the production of toluene from biomass-derived furans, good yield (65%) could be reached. Compared to the Brønsted acid zeolites, H-beta or H-Y, the formation of coke on the surface of the combined system of Lewis acid ($AlCl_3$) + zeolite (Na–Y) was less significant probably due to the retarded oligomerization of 2-MF.[21] Meanwhile, despite its lower acid strength, H-[B]-BEA showed an activity similar to the H-[Al]-BEA in the production of benzene and *p*-xy from furan and 2,5-DMF. A three-in-one reaction, Diels–Alder cycloaddition of 2,5-DMF with acrylic acid, dehydration to form the phenyl-ring, and final decarboxylation to *p*-xylene, was reported by Mendoza Mesa *et al.*[22] Therein, a complete 2,5-DMF conversion with a *p*-xy yield of 83% was achieved using a H-beta zeolite at 473 K in a continuous flow system. In this case, the use of acrylic acid, which is considered an activated dienophile for the Diels–Alders reaction, explains the high aromatic production achieved compared to results attained when non-activated olefins (*i.e.* ethene, propene) are used. Analysis with a microkinetic model revealed that, even with this weaker acidity, the dehydration reaction is sufficiently catalyzed, activating the aromatic production pathway.[23] Considering these reports, it is important to note that most of the industrial or semi-industrial (pilot plants) processes to produce aromatics from biomass-derived furans involve the use of zeolites as catalysts.[24] However, the main drawback of their use is the rapid deactivation they suffer due to the deposition of coke promoted by their high activity and Br/Le acidity, as well as their small pore size.[2,25] In this sense, silica–alumina aerogel was reported as a highly active catalyst for *p*-xy production which could be attributed to its high surface area, large mesoporous volume and high acid sites concentration, in particular Br acid sites; this feature could indicate that the overall rate of *p*-xy production is limited by the dehydration of the cycloadduct.[26]

Although interesting results have been reported on the subject, the production of aromatic compounds from biomass-derived furans is still a challenging process since the most active catalysts such us zeolites are easily deactivated by trapping oligomeric species inside their pores. To address these limitations, tailoring the relation between Br and Le sites of different strength on a mesoporous matrix can be an interesting strategy to enhance the DA reaction of biomass-derived furans and the further cycloadduct dehydration towards the aromatic production.

Following this idea, in this work the design and synthesis of acid catalysts based on SBA-15 mesoporous silicates, which present as advantages their higher sizes and volumes of pores as well as high specific surface suitable for functionalization, is proposed. Such features lead to expect a

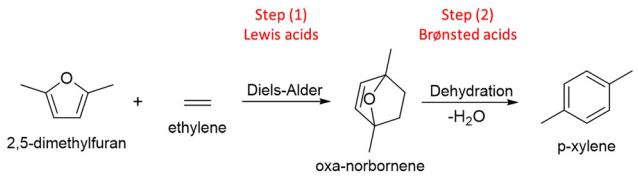

Scheme 1 Two stages process for the synthesis of aromatics (*p*-xylene, *p*-xy) from 2,5-DMF and olefins.

better accessibility and interaction of the reactive molecules with active sites generated from the excellent versatility of these materials for their functionalization according to the desired application. The modification of the silicate structures by incorporating heteroatoms different from Si, such as Al, Ga, Zr, W, Nb, allows the development of different kind of acid sites, Le and/or Br, on the catalyst.[2,25,27,28] For this reason, applying SBA-15 mesoporous silicates modified with acid functions results a very interesting alternative barely explored yet to develop a route for the synthesis of renewable aromatic compounds through the catalytic conversion of biomass-derived furans. This study was particularly focused on the role of acid sites (Br and Le) and the nature of metals present in the catalysts and their influence on the observed catalytic behavior.

Experimental

Catalysts synthesis method

The mesoporous silicate with SBA-15 structure was synthetized using Pluronic 123 (P123) as structure director and tetraethoxysilane (TEOS) as Si precursor.[29] In a first stage of synthesis, P123 is dissolved at 40 °C in a 2 M solution of HCl, and thereafter TEOS was added. The stirring at 40 °C was started and maintained for 20 h, and then the obtained gel was submitted to hydrothermal treatment at 80 °C for 24 h. Then, the solid was washed until reach the pH of distilled water, filtered and dried at 60 °C for 12 h. Finally, the P123 was eliminated from the pores by calcination in air at 500 °C for 8 h.

In the case of modified SBA-15 solids, the next metal precursors were used: niobium(v) oxalate hydrate for Nb, ammonium metatungstate hydrate for W, zirconium(iv) oxide chloride for Zr, gallium(iii) nitrate hydrate for Ga and aluminium nitrate for Al. The synthesis procedure was:

- Monometallic solids: the corresponding precursor of Nb, W, Zr or Ga previously dissolved in water was added to the solution of P123 in 2 M HCl, stirred for 15 min, and then the TEOS was added. The gel was submitted to stirring at 40 °C for 20 h, and then to a hydrothermal treatment at 100 °C for 24 h. These solids were prepared from a nominal Si/M molar ratio of 20 and they were named as M(x)–S, where M corresponds to the metal incorporated in the structure and x to the real Si/M molar ratio obtained from ICP measurements. It is important to clarify that for Ga(∞)–S, between parenthesis is indicated the real Si/Ga molar ratio, showing this value that under the applied synthesis conditions, Ga was practically not incorporated in the structure.

- Monometallic of Al and bimetallic Al–M solids (where M is Nb, W, Zr or Ga): the source of Al together with the corresponding M source, previously dissolved in water, were added to the solution of P123 in 2 M HCl and stirred for 15 min; then TEOS was added and the stirring was continued for 1 h. The pH of gel was increased to 5 by using $NH_4(OH)$ solution and the stirring was maintained at 40 °C for 20 h. Finally, a hydrothermal treatment at 100 °C for 24 h was applied. These solids were prepared from a nominal Si/Al and Si/M molar ratio of 20. The solids were named as Al(x)–M(x)–S where M corresponds to the metal incorporated in the structure and x to the real Si/M or Si/Al molar ratio obtained from ICP measurements.

In order to study the influence of metal content for catalysts modified with Al and Nb, solids with different Si/Al and Si/Nb molar ratio were synthetized following the procedure applied for the synthesis of bimetallic solids. In this case a nominal Si/Al molar ratio of 20 was maintained and the Si/Nb was varied from 20, 40 and 60. In order to infer the influence of the initial Al content in the synthesis gel, a solid from a Si/Al molar ratio of 60 and Si/Nb of 20 was also tested. These solids were named as Al(x)–Nb(x)–S where x is the molar fraction X_{Al} or X_{Nb} calculated from the real Al and Nb molar content determined from ICP measurements as follows: $X_{Al} = n_{Al}/(n_{Al} + n_{Nb})$ and $X_{Nb} = n_{Nb}/(n_{Al} + n_{Nb})$ (where n_{Al} and n_{Nb} are the moles of each metal). Then, solid with an Al molar fraction from 0 to 1 could be analyzed.

Catalysts characterization

The synthetized solids were characterized by X-ray diffraction (XRD) (λ = 1.5418 Å) using a Panalytical–Empyrean diffractometer with PIXcel 3D detector in the range of 1–3° and 5–90° to confirm the mesoporous structural order development and the probable presence of metal oxide phases. N_2 adsorption isotherms were collected using a Micromeritics ASAP 2420 previously degassing the samples (200–300 mg with particle sizes between 0.4–0.8 mm) under vacuum overnight at 300 °C. Specific areas were calculated by the Brunauer–Emmett–Teller (BET) method, pore size distributions and pore volumes were obtained by the Barrett–Joyner–Halenda (BJH) method.

For textural characterization of samples, high resolution transmission electron microscopy (HR-TEM) measurements were performed using a JEOL JEM-2100F instrument working at 200 kV (point resolution of 0.17 nm).

With the aim of inquiring about the acid properties of solids, infrared spectra (FT-IR) of adsorbed pyridine were recorded on a Thermo Scientific Nicolet iS10 spectrometer following the procedure reported by Vaschetto *et al.*,[30,31] where self-supported wafers were degassed under vacuum (10^{-3} Pa) at 400 °C for 7 h. After cooling at room temperature, the spectrum of each sample was recorded to be used as the background spectra. Afterwards, pyridine was admitted until reach the saturation of system and maintained in contact for 12 h. Then, FT-IR spectra were acquired, and the subsequent spectra were recorder after pyridine desorption by evacuation for 1 h at 50 °C and 200 °C. The background spectrum was then subtracted from each spectrum and the absorbance was normalized to wafers weight before calculations. The concentration of acid sites was calculated from band intensities (signals at *ca.* 1545 and 1450 cm^{-1} for Br and Le sites, respectively) and extinction coefficients, applying a method previously proposed.[32]

The analysis of acid properties was complemented with temperature-programmed desorption of ammonia (TPD-NH_3) which was carried out in a Micromeritics TPD/2900 device. For this procedure, solids (100 mg with particle sizes between 0.4–0.8 mm) were treated at 350 °C for 1 h under He flow for the removal of adsorbed contaminants and volatile species. Afterwards, NH_3 chemisorption was performed by pulses at 100 °C until attaining the equilibrium. After this, samples were submitted to He flow for 15 min to eliminate physisorbed ammonia and then, temperature was increased about 10 °C min^{-1} up to 500 °C under 100 mL min^{-1} He flow. Desorbed ammonia was monitored by a thermal conductivity detector (TCD, Micromeritics) and by a mass spectrometer (MS, Micromeritics) following the NH_3 characteristic mass of 15 a.m.u. (atomic mass unit).

The chemical composition of solids was determined by inductively coupled plasma emission spectroscopy (ICP) using a Varian 715-ES ICP optical emission spectrometer (Agilent Technologies).

Carbon deposition on solids after reaction was determined by means of elemental analysis in a Euro EA 3000 elemental analyzer (EUROVECTOR).

Catalytic test on the aromatization reaction

The synthetized solids were tested on the aromatization reaction of 2,5-DMF with ethylene using a 12 ml autoclave reactor with an interior vessel of PEEK (polyether-ether-ketone), equipped with pressure and temperature controllers, a magnetic bar, and a valve for gas injection and/or sample collection. Typically, the solid catalysts screening was made by applying the following reaction conditions: 250 °C, pressurized with ethylene at 20 bar, with 150 mg of catalyst, 0.3 g of 2,5-DMF, and 1,4-dioxane as solvent, at 1000 rpm, during 6 h. After reaction, the reactor was cooled to room temperature and samples of gas and liquid phase were taken. The liquid phase was filtered off and diluted in 0.8 g of a standard solution (2 wt% of *n*-dodecane in isopropanol), and then analyzed by gas chromatography (GC) using a Bruker 430 GC equipped with an FID detector and a capillary column (TRB-624, 60 m length). The products in gas phase (C_2H_6, C_2H_4, CH_4, CO_2, CO, *etc.*) were quantified by GC using a Varian 450-GC chromatograph equipped with three detectors; two thermal conductivity detectors (TCD) for H_2 and N_2 analysis, separated in a Hayesep Q pre-column and Molsieve 13X column, respectively, and a flame ionization detector (FID) for C1–C6 hydrocarbons (propane, butane, pentane, hexanes, *etc.*) analysis, wich are separated in a Hayesep Q pre-column and a Al_2O_3 MAPD column. The presence of carbon as coke deposition on catalyst after reaction was determined by elemental analysis measurements (as above-mentioned). Carbon balance values for each catalytic test was calculated by totaling C (mol%) in liquid + gas + solid fraction obtained from reaction (see for example, Fig. S4 in ESI†). The catalytic results were exposed in terms of *p*-xy yield, *p*-xy-selectivity and 2,5-DMF conversion, and calculated as:

$$Y_{p\text{-xy}} = (\text{mols}_{p\text{-xy}}/\text{mols}_{2,5\text{-DMF}}) \times 100\%,$$

$$S_{p\text{-xy}} = (\text{mols}_{p\text{-xy}}/\text{mols of total product in liquid phase}) \times 100\%,$$

$$X_{2,5\text{-DMF}} = [(\text{mols}_{2,5\text{-DMF0}} - \text{mols}_{2,5\text{-DMFi}})/\text{moles}_{2,5\text{-DMF0}}] \times 100\%.$$

Some preliminary catalytic tests were performed to evaluate two main operational parameters as the stirring rate and the catalyst particle diameter, and results in terms of 2,5-DMF conversion and selectivity to *p*-xylene, as well as calculated reaction rates (mols converted per min) are summarized in Fig. S7 and S8 in ESI.† The thus obtained data demonstrated that the system works without any diffusional limitation under the reaction conditions employed in this study.

Results and discussion

Different acid catalysts based on SBA-15 mesoporous silicates functionalized by incorporating heteroatoms different from Si, such as Al, Ga, Zr, W, Nb in the structure were synthesized, and then well characterized by different techniques for solids analysis.

Fig. S1 in ESI† shows the SBA-15 SAXS pattern in which the presence of peaks corresponding to ($d_{1\ 0\ 0}$), ($d_{1\ 1\ 0}$) and ($d_{2\ 0\ 0}$) diffraction planes characteristic of p6mm hexagonal symmetry of SBA-15 pore arrangement.[33,34] Fig. 1 shows the XRD patterns corresponding to all synthesized materials. Here it should be clarified that, although the peak corresponding to ($d_{1\ 0\ 0}$) plane could not be detected because of the operability limit of XRD diffractometer detector, the presence of the two peaks emerging at higher angles, ($d_{1\ 1\ 0}$) and ($d_{2\ 0\ 0}$), confirmed the development of the hexagonal ordering typical SBA-15 structures.[35] It is interesting to note that after metals incorporation in the synthesis gel, the pore structure was maintained. Nevertheless, some distortions can be observed due to the differences in the metal cation size, oxidation state and their interaction with the structure. This feature is more pronounced for Al(17)–Ga(26)–S and Al(18)–W(817)–S samples. High angle XRD patterns (see Fig. S1 in ESI†) lack peaks corresponding to the presence of metallic phases, indicating that if these were formed should have a particle size smaller than 9 nm.[29]

As it was above-mentioned, the aromatization reaction here studied have two main stages or pathways (see Scheme 1): in the first step an oxanorbornene-type DA cycloadduct is formed by DA cycloaddition of 2,5-DMF and ethylene; meanwhile the second stage consists in the dehydration of DA cycloadduct to produce the aromatic. These stages could be catalyzed by the presence of Le and Br acid sites, respectively. In addition, several side reactions could be catalyzed by the presence of acids with the consequent formation of different byproducts, such as ketones, aldehydes, and larger polymerized byproducts.[23] These last substances are difficult to characterize or quantify experimentally by GC and could be trapped in the pore structure resulting in coke formation and further catalyst

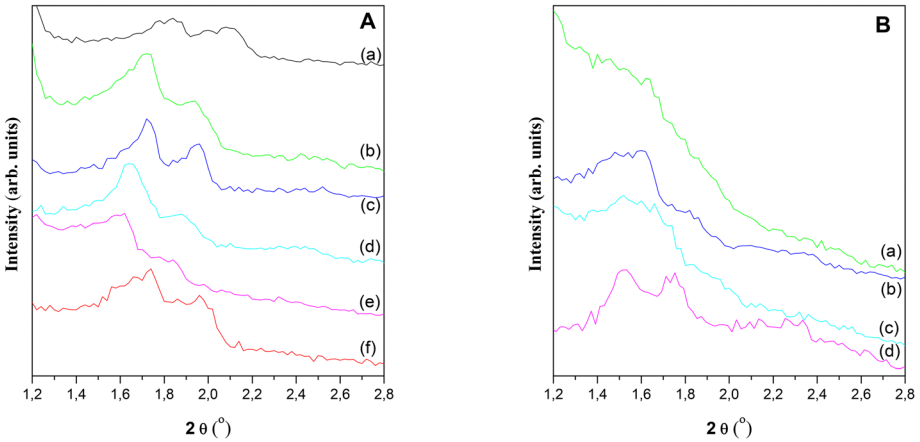

Fig. 1 Low angle XRD patterns of A) SBA-15 (a), Ga(∞)–S (b), Nb(77)–S (c), W(1020)–S (d), Zr(28)–S (e), Al(17)–S (f), and B) Al(17)–Ga(26)–S (a), Al(117)–Nb(20)–S (b), Al(18)–W(817)–S (c), Al(17)–Zr(20)–S (d).

deactivation. Taking in mind that the major limitation of the zeolites for this process is their deactivation by coke deposition, the synthesized mesoporous catalysts can be very promising if the optimization of their acid properties is reached in order to enhance the *p*-xy yield. Therefore, the acid properties were analyzed by pyridine (Py) chemisorption followed by FT-IR spectroscopic measurements. This technique has the notable advantage that the used basic molecule of Py can interact differently with Le and Br acid sites giving rise to characteristic bands in the FT-IR spectra.[29] On the other hand, the acid strength can be inferred considering the presence and intensity of the bands after Py desorption at different temperatures. Data reported in Table 1 correspond to the quantification of Le and Br sites in the synthetized solids after desorption of Py at two different temperatures. The sites present after desorption at 50 °C are considered a mixture of weak and moderate strength, meanwhile the sites still present after desorption at 200 °C are considered of moderate strength. Additionally, the metal contents of the samples obtained from ICP measurements are reported in Table 1.

Fig. 2A displays the results of catalytic tests exposed in terms of 2,5-DMF conversion (X_{DMF}), *p*-xy yield ($Y_{p\text{-xy}}$) and *p*-xy selectivity ($S_{p\text{-xy}}$) for each one of the acid catalysts here prepared. Meanwhile, in Fig. 2B the bars indicate the moderate Br/Le site. On one hand, 2,5-DMF conversion (X_{DMF}) and *p*-xy production for monometallic catalysts containing Ga, Nb and W were very low comparing with those incorporating Zr and Al in the SBA-15 structure, respectively; the best results being attained with Al(17)–S catalyst yielding close to 20% of *p*-xy. On the other hand, bimetallic samples offered better furan reactant conversion (X_{DMF}) and *p*-xy yield ($Y_{p\text{-xy}}$), where the Al(117)–Nb(20)–S catalyst reached the best *p*-xy production (25% yield).

From the acidity measurements (data reported in Table 1) it could be observed that monometallic solids modified with Ga, Nb or W only showed Le acid sites of weak strength (a high proportion are not present for desorption at 200 °C). Instead, when Al or Zr was incorporated, the solids showed the presence of Le and also Br acid sites. In fact, only these last catalysts (with both Br and Le acid sites) presented an interesting behavior in the tested reaction reaching a *p*-xy

Table 1 Metal content (wt%) in the synthesized solids and acid sites quantification (in $mmol_{Py}$ g^{-1} catalyst) determined by FT-IR spectroscopy (after desorption at 50 and 200 °C)

	Metal content (wt%)		Acid sites ($mmol_{Py}$ g^{-1} of catalyst)				Br/Le ratio	
			Br		Le			
Catalyst	Al	M[a]	50 °C	200 °C	50 °C	200 °C	50 °C	200 °C
Ga(∞)–S	—	0.004	0.00	0.00	0.34	0.01	0.01	0.20
Nb(77)–S	—	1.56	0.01	0.00	0.56	0.02	0.01	0.32
W(1020)–S	—	0.26	0.00	0.00	0.44	0.01	0.01	0.20
Zr(28)–S	—	4.17	0.04	0.03	0.33	0.07	0.13	0.44
Al(17)–S	2.08	—	0.32	0.08	0.50	0.10	0.63	0.78
Al(17)–Ga(26)–S	2.02	3.54	0.10	0.07	0.27	0.15	0.39	0.45
Al(117)–Nb(20)–S	0.35	7.13	0.10	0.05	0.30	0.05	0.35	0.99
Al(18)–W(817)–S	1.97	0.30	0.13	0.06	0.34	0.09	0.37	0.65
Al(17)–Zr(20)–S	1.98	5.56	0.14	0.07	0.33	0.11	0.42	0.64

[a] wt% of the incorporated metal (Ga, Nb, W or Zr) in the SBA-15 structure measured by ICP.

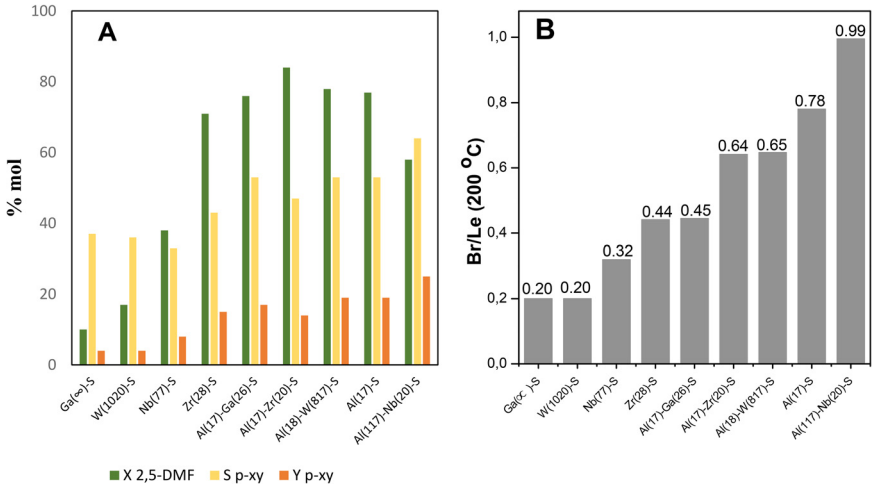

Fig. 2 A) Catalytic activity in terms of 2,5-DMF conversion ($X_{2,5\text{-DMF}}$), *p*-xylene selectivity ($S_{p\text{-xy}}$) and *p*-xylene yield ($Y_{p\text{-xy}}$), for the different catalysts. B) Br/Le ratio of sites with moderate strength (from IR data with pyridine desorption at 200 °C) measured for each catalyst. Data ordered in function of increasing Br/Le ratio.

yield ($Y_{p\text{-xy}}$) near to that observed for H-ZSM-5 (20% of $Y_{p\text{-xy}}$, see Table S1 in ESI†), which is the catalyst commonly used in aromatization reported processes and taken as a reference in this work. It is important to mention that furan derivatives are susceptible to be affected by hydrolysis reactions when acids are present and, consequently, an important by-product is usually formed from the furan ring hydrolysis, the diketone hexanedione, which could further undergo polymerization reactions.[36] Thus, the yield to hexanedione should be also determined in each catalytic test. Interestingly, solid modified with Nb showed a high selectivity to hexanedione (47% in liquids) and a hexanedione yield of 11% with respect to values between 4 and 8% observed for the other catalysts (see data in Table S1 in ESI†). From these results it could be inferred that among monometallic solids those with high Br/Le ratio were efficient for the *p*-xy production. In order to enhance the Br/Le ratio of these metal incorporated on SBA-15 structure (M-S) catalysts, bimetallic solids were also synthesized incorporating Al (that ensures the Br acidity) together with other metal (Ga, Nb, W or Zr) in the mesoporous material.

Comparison between mono- and bi-metallic solid catalysts here studied evidence that, although the amount of Le sites predominantly weak is slightly higher than that of Br sites for all of solids (ratio of Br/Le < 1), the bimetallic solids show an increase in the amount of Br sites and increased Br/Le ratios (see Table 1). Nevertheless, from the catalytic results exposed in Fig. 2 it can be observed that only those bimetallic catalysts showing the higher moderate Br/Le ratios (see Table 1) display the major selectivity and yield to *p*-xy; this feature evidences a clear dependence of the catalytic efficiency with the type and strength of acid sites present in the catalysts. In this sense, the Al(117)–Nb(20)–S material with the highest moderate strength Br/Le ratio (0.99) gave the higher *p*-xy production ($Y_{p\text{-xy}}$ = 25%). Moreover, Al(17)–Zr(20)–S showed an increased 2,5-DMF conversion along with decreased selectivity and yield of *p*-xy with respect to Al(117)–Nb(20)–S. This Zr and Al modified solid showed high amounts of both types of acid sites (see Table 1) with a moderate Br/Le ratio of 0.64 (lower than that of the Al–Nb bimetallic system). Therefore, it is probable that the lower proportion of moderate strength Br acid sites results in the lower probability of cycloadduct dehydration, thus provoking the *p*-xy production decrease observed in this case.

From the results up to now attained it could be concluded that the nature (Br and/or Le) and the strength (moderate or week) of the acid sites present in the here studied catalysts are essential for the occurrence of the two steps aromatization reaction to produce selectively *p*-xy from 2,5-DMF and ethylene. Nevertheless, there exist other parameters in the solid catalyst to take into consideration, such as the distribution of the acid sites in the mesoporous material. Thus, the specific surface, pore volume and diameter of the bare SBA-15, Al–S(17) and bimetallic solids (Al–M) here prepared were determined from N_2 physisorption measurements. All the N_2 adsorption isotherms attained (see Fig. S2 in ESI†) are type IV indicating the presence of mesoporosity, as expected. The obtained parameter values were according with the development of a hexagonal pore arrangement typical of SBA-15 structures (see Table 2) giving account for the interesting properties of these solids to be used as heterogeneous catalysts. Therefore, it is expected an enhanced interaction between the catalytic active sites present in the structures with the reactant molecules. In this sense, the catalyst showing the highest *p*-xy yield (SBA-15 modified with Al and Nb) is that showing the lowest surface density of total moderate acid sites (number of Br and Le sites or total acid sites per surface of solid, Table 2 and Fig. 3) and the higher intrinsic catalytic activity ($mmol_{p\text{-xy}}$ per surface density of total moderated acid sites, Table 2). This fact evidences that a high acid sites dispersion in the catalyst

Table 2 Main textural properties (specific surface area, pore diameter and pore volume) obtained from N_2 physisorption measurements and calculated surface density of total moderate acid sites and intrinsic catalytic activity for catalysts

Catalyst	Surface area[a] ($m^2\ g^{-1}$)	P_D[b] (nm)	P_V[c] ($cm^3\ g^{-1}$)	Surface density of total moderate acid sites[d] ($mmol_{py}\ m^{-2}$)	Intrinsic catalytic activity[e]
SBA-15	578	5.84	0.70	—	—
Al(17)–S	725	6.57	1.00	2.48×10^{-4}	7.6×10^4
Al(17)–Ga(26)–S	601	8.48	1.13	3.66×10^{-4}	4.6×10^4
Al(117)–Nb(20)–S	558	9.90	1.23	1.79×10^{-4}	1.4×10^5
Al(18)–W(817)–S	733	7.52	1.20	2.05×10^{-4}	9.2×10^4
Al(17)–Zr(20)–S	565	8.03	1.07	3.19×10^{-4}	4.3×10^4

[a] Specific surface area calculated by BET method. [b] Pore diameter. [c] Pore volume calculated from BJH adsorption branch. [d] Data obtained from FT-IR of adsorbed pyridine. [e] $mmol_{p\text{-xy}}$ per surface density of total moderated acid sites.

surface and a high accessibility to the acid sites could consequently reinforce its efficiency as catalytic site for the tested reaction. Moreover, modified SBA-15 mesoporous materials have pore diameters (P_D) in a narrow range between 5.80 and 9.90 nm and quite similar pore volumes (P_V) ranging between 0.70 and 1.23, respectively. Interestingly, the highest values of P_D and P_V correspond to the best catalyst Al(117)–Nb(20)–S here studied. Therefore, the here designed Al–Nb-SBA-15 mesoporous materials offers a higher accessibility to their acid sites, and, consequently, a higher efficiency during the aromatization process with lower sub-products formation when comparing with for example zeolitic materials commonly used in this process, which present microporous frameworks with much lower accessibility to active sites and some diffusional drawbacks (see Table S1 in ESI†).

From TEM images of Al(117)–Nb(20)–S sample, taken as reference (Fig. 4), it could be observed the presence of highly ordered mesoporous structures of unidirectional meso-channels. In these images, the presence of segregated oxide nanoparticles of Nb or Al is not detected, this fact confirming the high dispersion of the metal species on the catalyst surface. From image c, a pore diameter of around 8.5 nm could be measured which agrees with the value estimated from N_2 physisorption measurements (see Table 2).

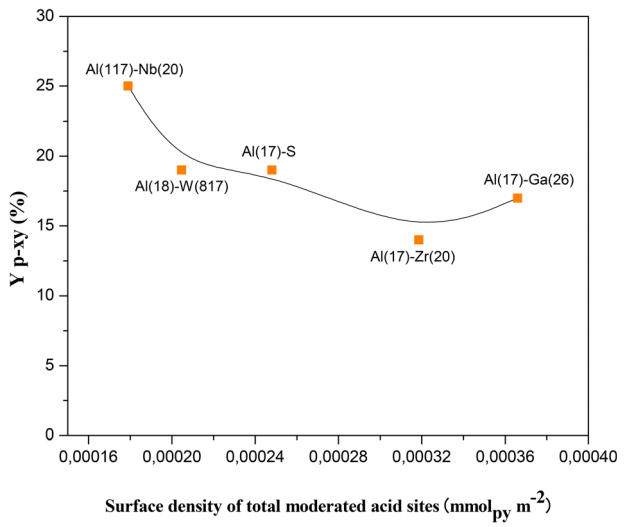

Fig. 3 Yield to *p*-xylene ($Y_{p\text{-xy}}$) as a function of the surface density of total moderate acid sites (number of moderate Br and Le acid sites per surface of solid).

Taking into account that the bimetallic catalyst modified with Al and Nb [Al(117)–Nb(20)–S] showed the best results in terms of *p*-xy production, solids with different Si/Al and Si/Nb ratios were synthesized to analyze the impact of metal contents can have on the acidity of the material and, consequently, on the catalytic behavior. Table 3 presents the metal contents determined by ICP, as well as the acid sites quantification for Al–Nb bimetallic catalysts synthesized with different Al and Nb contents.

The prepared Al–Nb bimetallic catalysts were tested in the aromatization reaction of 2,5-DMF with ethylene for the selective *p*-xylene production, and the results of the catalytic tests are shown in Fig. 5A, where an interesting behavior for solids with different Al and Nb contents can be observed. For its part, in Fig. 5B, it is shown the Br/Le ratio of moderate strength sites. It was verified that presence of Al is sufficient to develop active catalysts for the aromatization reaction. Nevertheless, as the Nb incorporation in the structure increases (up to molar fraction = 0.85), a better activity in terms of selectivity ($S_{p\text{-xy}}$) and yield ($Y_{p\text{-xy}}$) to *p*-xy is achieved. This catalytic behavior could be explained by analyzing not only the amount and strength of acid sites but also the balance among them. Thus, a relationship between catalytic activity *vs.* the moderate strength Br/Le ratio can be found (see Fig. 6). Then, *p*-xy yield reached a maximum value for Al(0.15)–Nb(0.85)–S material [similar to Al(117)–Nb(20)–S sample of the series previously studied], which shows a moderate Br/Le ratio of ≈1 (Fig. 6). Instead, Al(0.7)–Nb(0.3)–S solid with a higher amount of Br acid sites and an increased moderate Br/Le ratio (≈1.4) showed a major 2,5-DMF conversion but a lower selectivity and yield to *p*-xy with respect to Al(0.15)–Nb(0.85)–S. These results allow inferring that the formation of *p*-xy is not favored by a greater proportion of Br than Le sites, which would be expected by considering that the two stages of the reaction mechanism for the aromatic compounds formation *via* DA reaction requires the presence of both Le and Br sites of moderate strength in adequate combination.

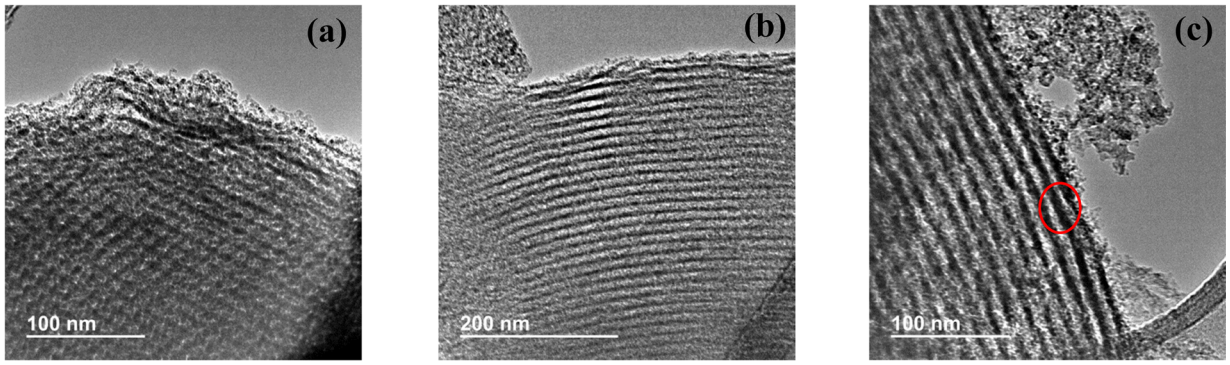

Fig. 4 TEM images of the Al(117)–Nb(20)–S ordered mesoporous material obtained with different magnification: at 100 nm (a) and 200 nm (b) scales, and pore diameter visualization (c).

Table 3 Effect of Al and Nb contents in catalysts on the acidity quantified by adsorbed Py ($mmol_{Py}$ g^{-1} of catalyst) after desorption at different temperatures (50 and 200 °C)

	Metal content (wt%)		Acid sites ($mmol_{Py}$ g^{-1} catalyst)				Total acid sites ($mmol_{Py}$ g^{-1} of catalyst)		Br/Le ratio	
			Br		Le					
Catalyst[a]	Al	Nb	50 °C	200 °C	50 °C	200 °C	50 °C	200 °C	50 °C	200 °C
Al(1)–Nb(0)–S	2.08	—	0.317	0.076	0.503	0.097	0.820	0.173	0.629	0.780
Al(0.70)–Nb(0.3)–S	1.38	2.06	0.126	0.063	0.301	0.045	0.427	0.108	0.419	1.383
Al(0.53)–Nb(0.47)–S	1.22	3.74	0.138	0.067	0.315	0.081	0.453	0.148	0.437	0.826
Al(0.15)–Nb(0.85)–S	0.35	7.13	0.104	0.049	0.297	0.049	0.401	0.097	0.352	0.994
Al(0.02)–Nb(0.98)–S	0.04	6.01	0.156	0.096	0.244	0.103	0.400	0.199	0.640	0.932
Al(0)–Nb(1)–S	0	1.57	0.005	0.005	0.564	0.015	0.569	0.020	0.010	0.320

[a] In parentheses is shown the molar fraction of incorporated metals according to: $X_{Al} = n_{Al}/(n_{Al} + n_{Nb})$ and $X_{Nb} = n_{Nb}/(n_{Al} + n_{Nb})$.

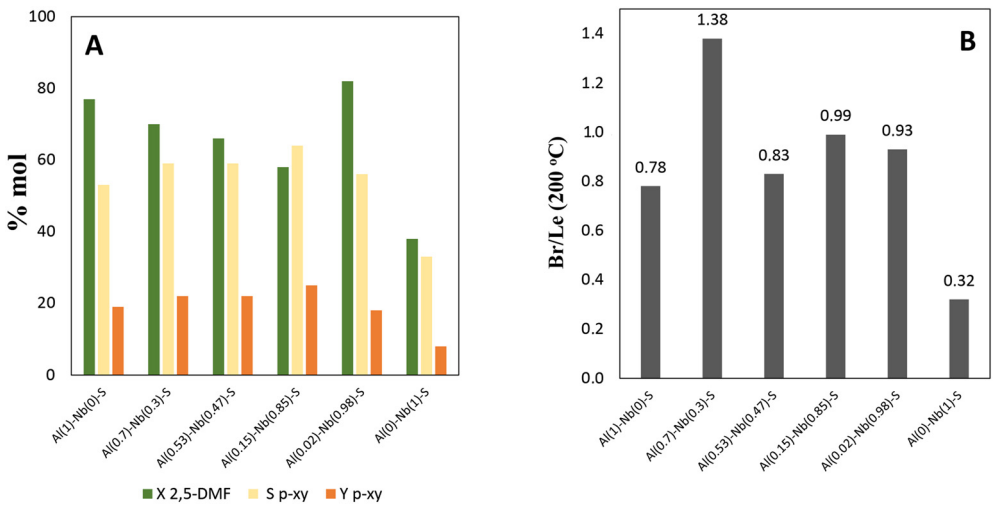

Fig. 5 A) Catalysts activity in terms of: *p*-xylene yield ($Y_{p\text{-xy}}$), *p*-xylene selectivity ($S_{p\text{-xy}}$,) and 2,5-DMF conversion ($X_{2,5\text{-DMF}}$), and B) moderate Br/Le ratio for all catalysts.

On the other hand, when Br/Le ratio is slightly lower than 1, but the amount of Al is too low (Al(0.02)–Nb(0.98)–S), the catalyst efficiency notably decreases. This fact evidences the importance of the nature of the metal incorporated in the SBA-15 structure for the *p*-xy production, also corroborating the need of a minimum Al content in the catalyst to favor the aromatization reaction. Finally, for Al(0)–Nb(1)–S catalyst only modified by Nb, which shows the predominant presence of weak Le acid sites, a poor catalytic activity with an increasing production of hexanedione was observed. Probably, the scarcity of Br acid sites for dehydration of the cycloadduct could shift the equilibrium to hexanedione production (see

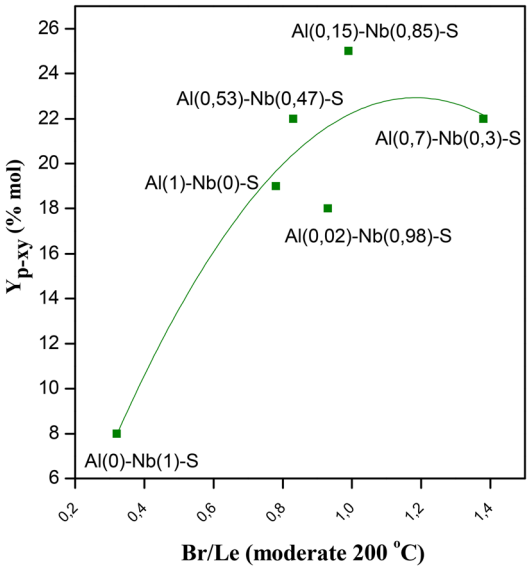

Fig. 6 *p*-xy yield as a function of moderate Br/Le ratio.

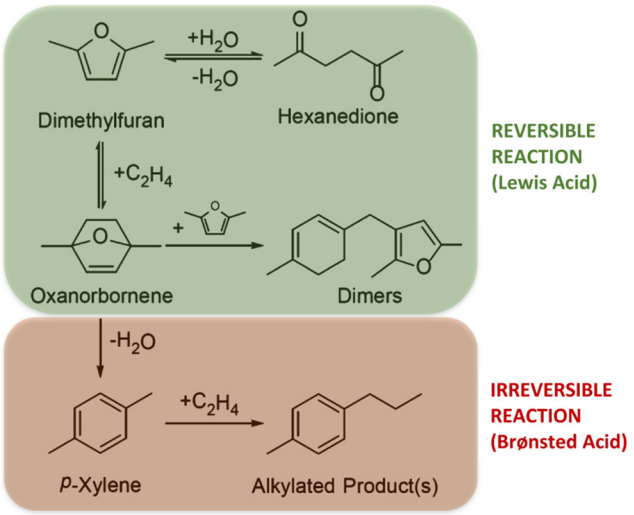

Scheme 2 Products and by-products obtained from the aromatization reaction of 2,5-DMF and ethylene during the different reaction stages catalyzed by Le or Br acid sites.

Scheme 2).[36] The carbon balance of catalytic experiments are shown in Fig. S4 in ESI.†

From catalytic results depicted in Fig. 5 and 6 and considering the acidity values measured for the materials (see Table 2), it is clear that the total acidity of the catalysts is not the main parameter guiding the catalytic behaviour, while the presence of an adequate combination of Br and Le acid sites of moderate strength (well dispersed and homogeneously distributed in the solid, this meaning with low surface density of acid sites) becomes essential to produce *p*-xy selectively. In order to corroborate the relationships encountered between catalytic activity and acid properties of the materials, the acidity of the series of catalysts was also determined by means of temperature programmed desorption of ammonia (NH_3-TPD), and the obtained results are given in Table 4 (and in Fig. S3 in ESI†). As can be seen, and in agreement with the Py adsorption/desorption measurements by FT-IR, the catalyst offering the better yields of *p*-xy ($Y_{p\text{-}xy}$ = 25%) does not have the higher total acidity measured by NH_3-TPD (225 mmol NH_3 per g solid), while other catalysts possessing higher total acidity values do not produce higher yields of *p*-xy (see Table 4).

Once the best Al–Nb bimetallic catalyst in the aromatization process was selected, optimization of the main reaction parameters, such as reaction temperature, ethylene pressure, catalyst and reactive concentration was made to enhance *p*-xy production. Fig. 7 shows the dependence of *p*-xy yields on temperature. When the temperature decreases, the yield to *p*-xy also decreases, reaching values similar to that of hexanedione, the main by-product. This is also reflected in the selectivity towards *p*-xy, which increases when increasing temperature reaching around 65% at 250 °C. This behavior agrees with that cited in the literature, since the DA reaction is mainly promoted by thermal activation (typically temperatures above 200 °C are used). Thus, since the cycloaddition is an endergonic reaction and the dehydration reaction is highly exergonic, the coupling of the strongly exothermic and entropically favored aromatization compensates the unfavorable DA equilibrium, providing the thermodynamic driving force for *p*-xy formation (Scheme 2).[37,38] Moreover, the hexanedione formed as by-product in the first stage of the of the process can reversibly convert back into 2,5-DMF to be further converted into *p*-xy (irreversible reaction), and therefore, as the conversion of 2,5-DMF increases, the thermodynamics of the system reduces the presence of hexanedione found in solution and helps drive it

Table 4 Effect of Al and Nb contents in catalysts on the total acidity quantified by NH_3-TPD measurements

Catalyst[a]	Metal content (wt%)		Total acidity (μmol NH_3 per g solid)	Yield to *p*-xy ($Y_{p\text{-}xy}$, %)
	Al	Nb		
Al(1)–Nb(0)–S	2.08	—	210	19
Al(0.70)–Nb(0.3)–S	1.38	2.06	237	22
Al(0.53)–Nb(0.47)–S	1.22	3.74	259	22
Al(0.15)–Nb(0.85)–S	0.35	7.13	225	25
Al(0.02)–Nb(0.98)–S	0.04	6.01	323	16
Al(0)–Nb(1)–S	0	1.57	43	8

[a] In parentheses is shown the molar fraction of incorporated metals according to: $X_{Al} = n_{Al}/(n_{Al} + n_{Nb})$ and $X_{Nb} = n_{Nb}/(n_{Al} + n_{Nb})$.

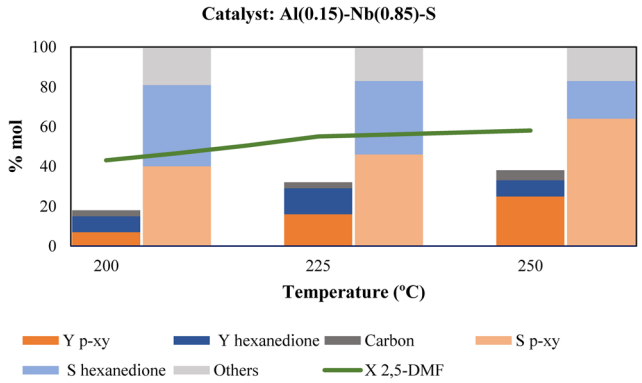

Fig. 7 Influence of temperature on the catalytic activity in terms of yield and selectivity to *p*-xylene and hexanedione, 2,5-DMF conversion and carbon % (measured by EA on the recovered catalyst after reaction). Reaction conditions: 20 bar of ethylene, 0.15 g of catalyst, 0.3 g of 2,5-DMF, 1,4-dioxane as solvent, 5 h of reaction time and magnetic stirring at 1000 rpm.

to high yields and selectivity to *p*-xy.[39] In addition, carbon deposited on the catalyst after each reaction was determined by means of elemental analysis (EA). As it can be observed in Fig. 7, the percentage of carbon was quite similar for the three tested temperatures and, in principle, it would not affect the catalyst activity.

As it can be seen in Fig. 8, an increase in ethylene pressure produce a major 2,5-DMF conversion, since by increasing the pressure of the system the dissolution of the gas in the liquid phase of 2,5-DMF and solvent also increases. This fact favors the interaction of the substrates with the catalyst[16] and shifts the equilibrium towards the desired product,[38] thus achieving the best yield to *p*-xy (32%) under a pressure of 30 bar of ethylene. The hexanedione yield did not vary significantly when the ethylene pressure was modified, while the better *p*-xy yield could be associated to its observed increased selectivity. Again, the amount of carbon deposited on the catalyst was quite similar for the different ethylene pressures essayed and it would not affect the catalytic activity observed.

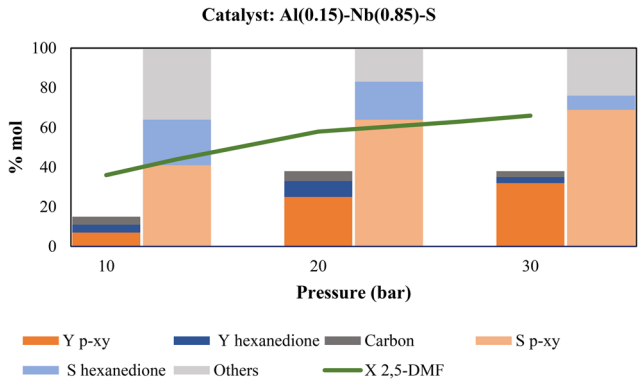

Fig. 8 Influence of ethylene pressure on the catalytic activity in terms of yield and selectivity to *p*-xylene and hexanedione, 2,5-DMF conversion and carbon % (deposited on used catalyst). Reaction conditions: 250 °C, 0.15 g of catalyst, 0.3 g of 2,5-DMF, 1,4-dioxane as solvent, 5 h of reaction time and magnetic stirring at 1000 rpm.

Following with the optimization of reaction parameters, two strategies were evaluated in order to increase the selectivity to *p*-xy: i) reducing by half the amount of catalyst or ii) reducing by half the concentration of 2,5-DMF. The results in Fig. S5† show that a decrease in the amount of catalyst caused a decrease in yield and selectivity to *p*-xy, while lower 2,5-DMF amount produced an increase in both values. According to Patet *et al.*,[39] with high catalyst concentration in the medium there are enough free active sites to catalyze the dehydration reaction (2nd step), and as a result, the DA reaction (1st step) becomes the rate-limiting. Meanwhile, when the catalyst concentration decreases, the dehydrative aromatization reaction becomes rate-limiting as a result of an insufficient number of active sites.[39] This agrees with the decrease in the yield of hexanedione when the amount of 2,5-DMF is decreased (column C), due to the increase in active sites for the aromatization of the cycloadduct. On the other hand, it is notable that the amount of water formed when the reaction is carried out with half of 2,5-DMF (0.52 mmol of water) is greater than that working with half the catalyst (0.43 mmol water). However, the catalyst is robust enough to favor *p*-xy selectivity over hexanedione. More importantly, by working under these reaction conditions (0.15 g of catalyst, 0.15 g of 2,5-DMF, column C in Fig. S5†) *p*-xylene yield of 34% is attained, while hexanedione yield and carbon deposited on catalyst are below 5%, respectively.

Once the above-mentioned reaction parameters were optimized, the influence of reaction time was evaluated, achieving the highest performance of the Al(0.15)–Nb(0.85)–S catalyst at 6 h of reaction (Fig. S6†). Probably, the 2,5-DMF/hexanedione equilibrium (see Scheme 2) after 2 h of reaction is shifted to 2,5-DMF, which is consumed during the irreversible aromatization reaction to generate the desired *p*-xy. As it can be seen, after 4 h of reaction, the selectivity to hexanedione strongly decreased, meanwhile the selectivity to *p*-xy increased from 60 to around 80%, this meaning that once the cycloadduct (and, consequently the 2,5-DMF) is transformed *via* dehydration to *p*-xy, the overall process takes place with relatively good efficiency.

In summary, optimization of the main reaction parameters of the aromatization reaction of 2,5-DMF with ethylene allows achieving high 2,5-DMF conversion (≈71%), *p*-xy selectivities (≈80%) and yields (48%) with low formation of hexanedione and other by-products and with very low carbon deposition on the solids (<5%), which strongly help to the stability of the catalyst during the process.

One of the main and advantageous characteristics of heterogeneous catalysts is the possibility of their reuse. To evaluate the performance of the Al–Nb-SBA-15 bimetallic catalyst in this regard, three different alternatives were considered once the solid catalyst is recovered after reaction: 1) reusing the catalyst without further treatment, 2) reusing the catalyst after washing with 1,4-dioxane or 3) reusing the catalyst after calcination in air at 500 °C. In all the cases, carbon on catalyst was determined after each use to evaluate the

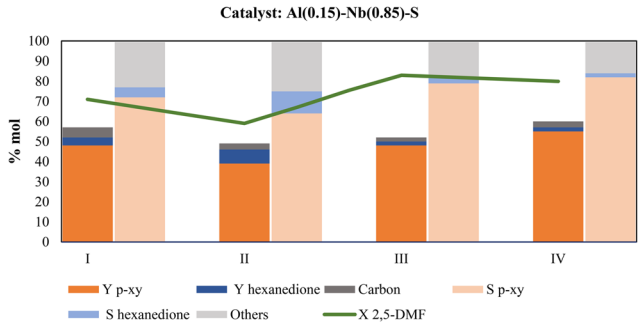

Fig. 9 Catalyst performance with respect to treatment applied before the re-use in terms of yield and selectivity to p-xylene and hexanedione, 2,5-DMF conversion, and carbon % (deposited on used catalyst). Fresh catalyst (column I), catalyst without treatment (column II), after washing with 1,4-dioxane (column III), and after calcination (column IV). Reaction conditions: 250 °C, 30 bar of ethylene, 0.15 g of catalyst, 0.15 g of 2,5-DMF and magnetic stirring of 1000 rpm.

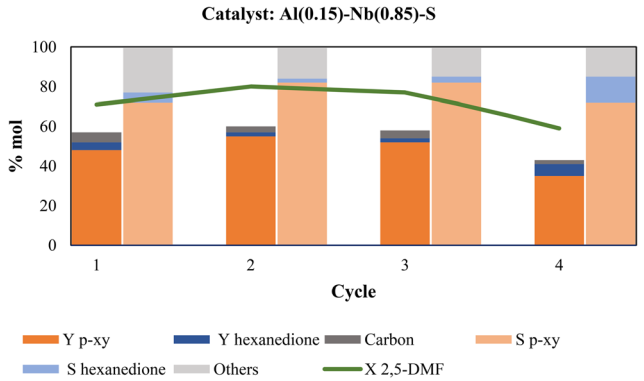

Fig. 10 Catalyst performance with consecutive reuses in terms of yield and selectivity of *p*-xylene and hexanedione, 2,5-DMF conversion and carbon % (deposited on used catalyst). Reaction conditions: 250 °C, 30 bar of ethylene, 0.15 g of catalyst, 0.15 g of 2,5-DMF and magnetic stirring of 1000 rpm.

carbonaceous matter deposition and its influence on catalyst activity during reuses. As it is shown in Fig. 9, the *p*-xy yield decreases from 48 to 39% when the catalyst is reused without any treatment (column II); however, after washing with 1,4-dioxane, the activity of the fresh catalyst (column I) is fully recovered (column III). Surprisingly, when the catalyst is subjected to calcination (column IV) an increase of 14% (from 48 to 55%) is observed in the *p*-xy yield with respect to the fresh catalyst used in the first catalytic test (column I). For this reason, this procedure was chosen to regenerate the catalyst and evaluate its reuse. In addition, the metal content of the catalysts was determined after each use, and the results are shown in Table 5. As can be seen, the metallic content remain practically constant independently of the type of treatment used after the recovery of the used catalyst and before the next reuse. These are very relevant results evidencing that the decay in the catalytic activity observed with treatment I (see Fig. 10) is not due to a metal loss from the solid. Probably, undesirable by-products like oligomers or polymers adsorbed on catalyst are responsible of the activity decreasing when the catalyst is not washed or calcined.

With the results of catalyst reuse depicted in Fig. 9 in mind, a new series of catalytic reuses was essayed by performing thermal regeneration of the used catalyst. Fig. 10 displays the catalytic behavior in function of various reaction cycles using calcination treatment to regenerate the catalyst. As can be seen, the *p*-xy yield was maintained above 50% during at least three consecutive cycles, while in the fourth cycle *p*-xy yield decreases by 27% (from 48 to 35%) compared to the first use of the fresh catalyst. As in the previous series of catalytic reuses, the metallic species present in the recovered catalyst of the four cycles were determined and the attained values provided in Table 6. As can be observed, the metal contents were maintained practically unaltered after three catalytic cycles; however, in the fourth cycle the Al and Nb contents decreased by 23% and 15%, respectively. As above-mentioned, the presence of Al in the catalyst is necessary to favor the aromatization reaction of 2,5-DMF, therefore a decrease in the Al content could reduce the *p*-xy yield. Nevertheless, our findings along this research work lead us to conclude that the presence of both Al and Nb metals in the SBA-15 mesoporous structure providing an adequate combination of Br and Le acid sites of moderate strength and homogeneously distributed on the solid (low surface density of acid sites), together with the high accessibility to these active sites offered by the mesoporous material, are the keys to attain active and effective catalysts for conducting the aromatization reaction of 2,5-DMF with ethylene to produce *p*-xylene selectively.

Table 5 Determination of Al and Nb contents for the catalysts after different treatments. I: after first use; II: reuse without treatment; III: reuse after washing; IV: reuse after calcination

	Catalyst treatment			
Content (wt%)	I	II	III	IV
Al	0.32	0.35	0.33	0.36
Nb	6.01	6.74	6.46	6.78

Table 6 Determination of Al and Nb contents for the catalysts after of each catalytic cycle (with thermal regeneration of the recovered/used catalyst)

	Cycle			
Content (wt%)	1	2	3	4
Al	0.32	0.36	0.35	0.27
Nb	6.01	6.78	6.64	5.64

Conclusions

The production of aromatics such as *p*-xylene from renewable blocks like ethylene and 2,5-DMF was achieved using metal modified catalysts based on SBA-15 structure. The best results were obtained with Al–Nb-SBA-15 bimetallic catalysts offering both Br and Le acid sites in adequate combination. The more promising catalyst was Al(0.15)–Nb(0.85)–S showing an optimal

ratio of Br/Le sites (with moderate strength) of around 1. The performance of this bimetallic catalyst, evaluated under optimized reaction conditions, such as temperature, ethylene pressure, catalyst and 2,5-DMF concentrations, displays a *p*-xylene yield of 48% with a *p*-xylene selectivity (in liquids) close to 80%. This catalyst showed a high specificity towards the main product, *p*-xylene, since only 2% of hexanedione yield was produced as the main by-product. Under these conditions, the catalyst could be used by at least three cycles without loss of activity. The stability an efficiency of the synthetized catalyst could be associated to the presence of Al and Nb metals in the mesoporous structure of SBA-15 silicates providing an adequate combination of Br and Le acid sites of moderate strength and highly dispersed on the solid (low surface density of acid sites), together with the high accessibility to these active sites offered by the mesoporous material. In this sense, this work employs materials engineering to synthesize bimetallic catalysts with specific Br/Le acid site ratios and controlled textural properties to improve the production of renewable *p*-xylene from biomass-derived furans and to extend the useful life of the catalyst with respect to current catalysts.

Conflicts of interest

There are no conflicts to declare.

Acknowledgements

Financial support by CSIC (Spain) through the project COOPB-20415 and the Spanish Government (MICINN, projects PGC2018-097277-B-I00 and PID2021-125897-B-I00) and by Argentinean Government through the project ANPCYT-PICT-2020-SERIEA-00918 are gratefully acknowledged. Authors also thank M. Parreño Romero and the Electron Microscopy Service of Universitat Politècnica de València for their support.

References

1 J. McGlone, P. Priecel, L. Da Vià, L. Majdal and J. A. Lopez-Sanchez, Desilicated ZSM-5 zeolites for the production of renewable p-xylene via diels–alder cycloaddition of dimethylfuran and ethylene, *Catalysts*, 2018, **8**, 253, DOI: **10.3390/catal8060253**.

2 A. E. Settle, L. Berstis, N. A. Rorrer, Y. Roman-Leshkóv, G. T. Beckham, R. M. Richards and D. R. Vardon, Heterogeneous Diels-Alder catalysis for biomass-derived aromatic compounds, *Green Chem.*, 2017, **19**, 3468–3492, DOI: **10.1039/c7gc00992e**.

3 M. Ventura, A. Marinas and M. E. Domine, Catalytic Processes for Biomass-Derived Platform Molecules Valorisation, *Top. Catal.*, 2020, **63**, 846–865, DOI: **10.1007/s11244-020-01309-9**.

4 H. Li, H. Guo, Z. Fang, T. M. Aida and R. L. Smith, Cycloamination strategies for renewable N-heterocycles, *Green Chem.*, 2020, **22**, 582–611, DOI: **10.1039/c9gc03655e**.

5 Z. Jiang, D. Hu, Z. Zhao, Z. Yi, Z. Chen and K. Yan, Mini-Review on the Synthesis of Furfural and Levulinic Acid from Lignocellulosic Biomass, *Processes*, 2021, **9**, 1234, DOI: **10.3390/pr9071234**.

6 R.-J. Van Putten, J. C. Van Der Waal, E. De Jong, C. B. Rasrendra, H. J. Heeres and J. G. De Vries, Hydroxymethylfurfural, A Versatile Platform Chemical Made from Renewable Resources, *Chem. Rev.*, 2013, **113**, 1499–1597.

7 Z. Moravvej, F. Farshchi Tabrizi and M. R. Rahimpour, RETRACTED ARTICLE: Vapor phase conversion of furfural to valuable biofuel and chemicals over alumina-supported catalysts: Screening catalysts, *Top. Catal.*, 2021, DOI: **10.1007/s11244-021-01470-9**.

8 B. C. Ledesma, J. M. Juárez, M. E. Domine and A. R. Beltramone, Influence of Ti incorporation to bimetallic mesoporous carbon in the production of 2,5-dimethylfuran from biomass derivatives, *Catal. Lett.*, 2022, **152**, 1530–1544, DOI: **10.1007/s10562-021-03711-8**.

9 M. Ventura, F. Nocito, E. de Giglio, S. Cometa, A. Altomare and A. Dibenedetto, Tunable mixed oxides based on CeO_2 for the selective aerobic oxidation of 5-(hydroxymethyl) furfural to FDCA in water, *Green Chem.*, 2018, **20**, 3921–3926, DOI: **10.1039/c8gc00972d**.

10 A. Corma, M. E. Domine and S. Valencia, Catalyst and catalytic process for the etherification/reduction of furfuryl derivatives to tetrahydrofurfuryl ethers, *WO Pat.*, 20144064318, 2014.

11 S. Kasipandi, J. M. Cho, K. S. Park, C. H. Shin and J. Woo Bae, Unprecedented activity and stability on zirconium phosphates grafted mesoporous silicas for renewable aromatics production from furans, *J. Catal.*, 2020, **385**, 10–20, DOI: **10.1016/j.jcat.2020.02.026**.

12 J.-F. Tremblay, MAKING AROMATICS IN SINGAPORE: Global consortium is building one of the world's largest p-XYLENE PLANTS in the city-state, *Chem. Eng. News*, 2011, **89**(38), 18–19, DOI: **10.1021/cen-v089n038.p018**.

13 P. C. A. Bruijnincx and B. M. Weckhuysen, Shale gas revolution: An opportunity for the production of biobased chemicals?, *Angew. Chem., Int. Ed.*, 2013, **52**, 11980–11987, DOI: **10.1002/anie.201305058**.

14 Z. Lin, V. Nikolakis and M. Ierapetritou, Alternative approaches for p-xylene production from starch: Techno-economic analysis, *Ind. Eng. Chem. Res.*, 2014, **53**, 10688–10699, DOI: **10.1021/ie402469j**.

15 K. C. Nicolaou, S. A. Snyder, T. Montagnon and G. Vassilikogiannakis, The Diels-Alder reaction in total synthesis, *Angew. Chem., Int. Ed.*, 2002, **41**, 1668–1698, DOI: **10.1002/1521-3773(20020517)41:10<1668::AID-ANIE1668>3.0.CO;2-Z**.

16 C. L. Williams, C. C. Chang, P. Do, N. Nikbin, S. Caratzoulas, D. G. Vlachos, R. F. Lobo, W. Fan and P. J. Dauenhauer, Cycloaddition of biomass-derived furans for catalytic production of renewable p-xylene, *ACS Catal.*, 2012, **2**, 935–939, DOI: **10.1021/cs300011a**.

17 K. N. Houk, F. Liu, Z. Yang and J. I. Seeman, Evolution of the Diels–Alder Reaction Mechanism since the 1930s: Woodward, Houk with Woodward, and the Influence of Computational Chemistry on Understanding Cycloadditions,

Angew. Chem., Int. Ed., 2021, **60**, 12660–12681, DOI: **10.1002/anie.202001654**.

18 C. C. Chang, S. K. Green, C. L. Williams, P. J. Dauenhauer and W. Fan, Ultra-selective cycloaddition of dimethylfuran for renewable p-xylene with H-BEA, *Green Chem.*, 2014, **16**, 585–588, DOI: **10.1039/c3gc40740c**.

19 E. Mahmoud, J. Yu, R. J. Gorte and R. F. Lobo, Diels-Alder and Dehydration Reactions of Biomass-Derived Furan and Acrylic Acid for the Synthesis of Benzoic Acid, *ACS Catal.*, 2015, **5**, 6946–6955, DOI: **10.1021/acscatal.5b01892**.

20 Y. P. Wijaya, H. P. Winoto, Y. K. Park, D. J. Suh, H. Lee, J. M. Ha and J. Jae, Heteropolyacid catalysts for Diels-Alder cycloaddition of 2,5-dimethylfuran and ethylene to renewable p-xylene, *Catal. Today*, 2017, **293–294**, 167–175, DOI: **10.1016/j.cattod.2016.12.032**.

21 Y. P. Wijaya, I. Kristianto, H. Lee and J. Jae, Production of renewable toluene from biomass-derived furans via Diels-Alder and dehydration reactions: A comparative study of Lewis acid catalysts, *Fuel*, 2016, **182**, 588–596, DOI: **10.1016/j.fuel.2016.06.010**.

22 J. A. Mendoza Mesa, F. Brandi, I. Shekova, M. Antonietti and M. Al-Naji, p-Xylene from 2,5-dimethylfuran and acrylic acid using zeolite in a continuous flow system, *Green Chem.*, 2020, **22**, 7398–7405, DOI: **10.1039/d0gc01517b**.

23 R. E. Patet, M. Koehle, R. F. Lobo, S. Caratzoulas and D. G. Vlachos, General Acid-Type Catalysis in the Dehydrative Aromatization of Furans to Aromatics in H-[Al]-BEA, H-[Fe]-BEA, H-[Ga]-BEA, and H-[B]-BEA Zeolites, *J. Phys. Chem. C*, 2017, **121**, 13666–13679, DOI: **10.1021/acs.jpcc.7b02344**.

24 *Biorizon Innovation and Upscaling of Renewable Aromatics Technology (BIO-HArT - Interreg)*, **https://www.biorizon.eu/bio-hart/**.

25 X. Feng, C. Shen, K. Ji, J. Yin and T. Tan, Production of p-xylene from bio-based 2,5-dimethylfuran over high performance catalyst WO3/SBA-15, *Catal. Sci. Technol.*, 2017, **7**, 5540–5549, DOI: **10.1039/c7cy01530e**.

26 Y. P. Wijaya, D. J. Suh and J. Jae, Production of renewable p-xylene from 2,5-dimethylfuran via Diels-Alder cycloaddition and dehydrative aromatization reactions over silica-alumina aerogel catalysts, *Catal. Commun.*, 2015, **70**, 12–16, DOI: **10.1016/j.catcom.2015.07.008**.

27 J. Yin, C. Shen, X. Feng, K. Ji and L. Du, Highly Selective Production of p-Xylene from 2,5-Dimethylfuran over Hierarchical NbOx-Based Catalyst, *ACS Sustainable Chem. Eng.*, 2018, **6**, 1891–1899, DOI: **10.1021/acssuschemeng.7b03297**.

28 R. Zhao, L. Xu, S. Huang and W. Zhang, Highly selective production of renewable: P -xylene from bio-based 2,5-dimethylfuran and ethylene over Al-modified H-Beta zeolites, Catal, *Sci. Technol.*, 2019, **9**, 5676–5685, DOI: **10.1039/c9cy01113g**.

29 V. R. Elías, P. A. Ochoa Rodriguez, E. G. Vaschetto, G. A. Pecchi, C. Huck-Iriart, S. G. Casuscelli and G. A. Eimer, Tailoring the stability and photo-Fenton activity of Fe-modified nanostructured silicates by tuning the metal speciation from different synthesis conditions, *Mol. Catal.*, 2020, **481**, 110217, DOI: **10.1016/j.mcat.2018.10.012**.

30 E. G. Vaschetto, G. a. Monti, E. R. Herrero, S. G. Casuscelli and G. a. Eimer, Influence of the synthesis conditions on the physicochemical properties and acidity of Al-MCM-41 as catalysts for the cyclohexanone oxime rearrangement, *Appl. Catal., A*, 2013, **453**, 391–402, DOI: **10.1016/j.apcata.2012.12.016**.

31 E. G. Vaschetto, S. G. Casuscelli and G. A. Eimer, Acidity versus catalytic activity in bi-structured nanomaterials, *Microporous Mesoporous Mater.*, 2018, **268**, 170–177, DOI: **10.1016/j.micromeso.2018.04.028**.

32 C. A. EMEIS, ChemInform Abstract: Determination of Integrated Molar Extinction Coefficients for IR Absorption Bands of Pyridine Adsorbed on Solid Acid Catalysts, *J. Catal.*, 1993, **141**, 347–354, DOI: **10.1002/chin.199338056**.

33 V. S. P. Ganjala, C. K. P. Neeli, C. V. Pramod, M. Khagga, K. S. R. Rao and D. R. Burri, Eco-friendly nitration of benzenes over zeolite-β-SBA-15 composite catalyst, *Catal. Commun.*, 2014, **49**, 82–86, DOI: **10.1016/j.catcom.2014.02.006**.

34 V. Elías, G. Ferrero, R. Oliveira and G. Eimer, Improved stability in SBA-15 mesoporous materials as catalysts for photo-degradation processes, *Microporous Mesoporous Mater.*, 2016, **236**, 218–227, DOI: **10.1016/j.micromeso.2016.09.001**.

35 D. Barrera, J. Villarroel-Rocha, L. Marenco, M. Oliva and K. Sapag, Non-hydrothermal synthesis of cylindrical mesoporous materials: influence of the surfactant/silica molar ratio, *Adsorpt. Sci. Technol.*, 2011, **29**, 975–988, DOI: **10.1260/0263-6174.29.10.975**.

36 Z. Li, Y. Jiang, Y. Li, H. Zhang, H. Li and S. Yang, Advances in Diels-Alder/aromatization of biomass furan derivatives towards renewable aromatic hydrocarbons, Catal, *Sci. Technol.*, 2022, **12**, 1902–1921, DOI: **10.1039/d1cy02122b**.

37 D. Wang, C. M. Osmundsen, E. Taarning and J. A. Dumesic, Selective Production of Aromatics from Alkylfurans over Solid Acid Catalysts, *ChemCatChem*, 2013, **5**, 2044–2050, DOI: **10.1002/CCTC.201200757**.

38 R. C. Cioc, M. Crockatt, J. C. van der Waal and P. C. A. Bruijnincx, The Interplay between Kinetics and Thermodynamics in Furan Diels–Alder Chemistry for Sustainable Chemicals Production, *Angew. Chem., Int. Ed.*, 2022, **61**(17), DOI: **10.1002/ANIE.202114720**.

39 R. E. Patet, N. Nikbin, C. L. Williams, S. K. Green, C. C. Chang, W. Fan, S. Caratzoulas, P. J. Dauenhauer and D. G. Vlachos, Kinetic Regime Change in the Tandem Dehydrative Aromatization of Furan Diels-Alder Products, *ACS Catal.*, 2015, **5**, 2367–2375, DOI: **10.1021/CS5020783/ASSET/IMAGES/CS-2014-020783_M003.GIF**.

